Frequency stabilization of distributed-feedback laser diodes at 1572 nm for lidar measurements of atmospheric carbon dioxide

Kenji Numata,[1,2,*] Jeffrey R. Chen,[2] Stewart T. Wu,[2] James B. Abshire,[2] and Michael A. Krainak[2]

[1]Department of Astronomy, University of Maryland, College Park, Maryland, 20742, USA

[2]NASA Goddard Space Flight Center, Greenbelt, Maryland, 20771, USA

*Corresponding author: kenji.numata@nasa.gov

Received 21 September 2010; accepted 17 December 2010;
posted 13 January 2011 (Doc. ID 135520); published 28 February 2011

We demonstrate a wavelength-locked laser source that rapidly steps through six wavelengths distributed across a 1572.335 nm carbon dioxide (CO_2) absorption line to allow precise measurements of atmospheric CO_2 absorption. A distributed-feedback laser diode (DFB-LD) was frequency-locked to the CO_2 line center by using a frequency modulation technique, limiting its peak-to-peak frequency drift to 0.3 MHz at 0.8 s averaging time over 72 hours. Four online DFB-LDs were then offset locked to this laser using phase-locked loops, retaining virtually the same absolute frequency stability. These online and two offline DFB-LDs were subsequently amplitude switched and combined. This produced a precise wavelength-stepped laser pulse train, to be amplified for CO_2 measurements.

OCIS codes: 350.6090, 300.6380, 140.3425, 280.1910.

1. Introduction

Carbon dioxide (CO_2) measurements from ice cores show that atmospheric CO_2 concentrations are higher now than they have been in the past 420,000 years [1]. It is becoming increasingly important to understand the nature and processes of the CO_2 sources and sinks, on a global scale, in order to make predictions of future atmospheric composition. Global measurements of the CO_2 mixing ratios from the Earth's orbit with 1 part per million by volume (ppmv) precision in the total column, 300 km spatial and monthly temporal resolution are needed to infer regional CO_2 terrestrial and oceanic sources and sinks in the presence of ~5 ppmv seasonal fluctuation [2–4]. Spaceborne measurements are required for the global coverage and spatial resolution that are not feasible with ground-based measurements [5]. The initial space-based CO_2 instruments [6,7] are passive spectrometers that use reflected sunlight as their light source. However, they have limited global coverage because they cannot measure at night or at low sun angles and can only measure over the ocean in a glint mode. Their measurements are also susceptible to biases from atmospheric scattering. The recent US National Research Council Decadal Survey for Earth Science [8] has recommended addressing the unmet needs in a laser-based NASA space mission called the Active Sensing of CO_2 Emissions over Nights, Days, and Seasons (ASCENDS). The laser-based approach for ASCENDS allows measurements of atmospheric CO_2 distributions with greater wavelength and spatial resolution during the day, night, and continuously over the ocean, allowing for global coverage.

A candidate lidar measurement approach for ASCENDS is currently being developed at NASA Goddard. It uses a nadir-viewing, integrated path differential absorption lidar (IPDA-DIAL) technique to measure the absorption of a single atmospheric CO_2 line in the column to the surface [9,10]. The lidar

0003-6935/11/071047-10$15.00/0

uses a pulsed laser that is stepped in wavelength across a single selected CO_2 line in a 1570 nm band. A direct detection receiver is used to record the time resolved laser backscatter profile from the atmosphere and surface. Postdetection analysis is used to isolate the echo pulses from the surface and determine the shape and optical depth of the atmospheric CO_2 line, from which the CO_2 column number density can be determined. The work summarized here demonstrates a precision laser seed source needed for the lidar's CO_2 transmitter.

A CO_2 line near 1572.335 nm was chosen for the measurement because of its suitable absorption strength, small temperature sensitivity, minimum interference from other species [11], and leverage of high-reliability 1.5 μm wavelength laser technology. Because atmospheric CO_2 has diurnal vertical transport, ideally the CO_2 column measurement needs to be uniformly sensitive to concentrations in the lower troposphere. This can be achieved by sampling the absorption at the sides of the line, where the absorption is from CO_2 molecules, which are pressure broadened in the lower troposphere [12]. The two-way transmittance of the 1572.335 nm CO_2 line from a 500 km orbit, shown in Fig. 1 (upper right corner), has a linewidth of ~3.3 GHz FWHM and steep slopes on the sides, making the measurements sensitive to laser frequency uncertainties. For this work, we used six measurement wavelengths, two offline and four on the sides of the line. However, the technique we describe is flexible and allows any number of wavelengths to be used. Generally, more wavelengths allow a higher resolution measurement of line shape.

The error contribution from the laser wavelength settings needs to be a small fraction of the total error budget to allow more margins for other error sources. To ensure 1 ppmv precision for CO_2 measurements near 1572 nm, an error budget of 0.08% is derived from an analysis of the sources of systematic errors. The frequency errors of online lasers need to be $< \pm$ 0.3 MHz to meet this target [13]. The frequency noise of an unlocked distributed-feedback laser diode (DFB-LD) is higher at lower frequencies and rolls off to a fixed low level above 100 kHz. The measurement error is averaged out within a pulse duration (~1 μs) for fast frequency noise above ~1 MHz, resulting in a minimum error contribution from fast frequency noise above 100 kHz. The measurement error can be further reduced from pulse-to-pulse averaging over a measurement averaging time (up to 10 s for spaceborne measurements). Error reduction from averaging diminishes for slower frequency drifts with periods longer than the measurement averaging time, therefore the present work focuses on methods for suppressing slow laser frequency drifts.

The basic design approach for the CO_2 sounder transmitter is illustrated in Fig. 1. The laser seeder (Fig. 1, left) serves as the master oscillator and defines spectral and temporal characteristics of the CO_2 transmitter. The seeder is rapidly stepped and switched among the six measurement wavelengths to provide the wavelength-stepped pulse train that is subsequently amplified by erbium-doped fiber amplifiers (EDFAs). All components along the optical train were polarization maintaining (PM) to avoid laser polarization drifts that may cause undesirable amplitude fluctuations in the measurements. The laser seeder for CO_2 falls into the telecom L-band, allowing us to use technologies developed by the telecom industry, which provides high performance and cost efficiency. We chose DFB-LDs as our laser oscillators to take advantage of their proven reliability. Rather than locking lasers directly to the side slopes of the absorption line, we employed an offset locking technique to tune slave lasers precisely to desired optical frequencies, up to $\pm$7 GHz away from that of a "master" laser. To do this, we have locked a master DFB-LD to 1572.335 nm CO_2 absorption line center (ν_0 in Fig. 1) and suppressed the peak-to-peak

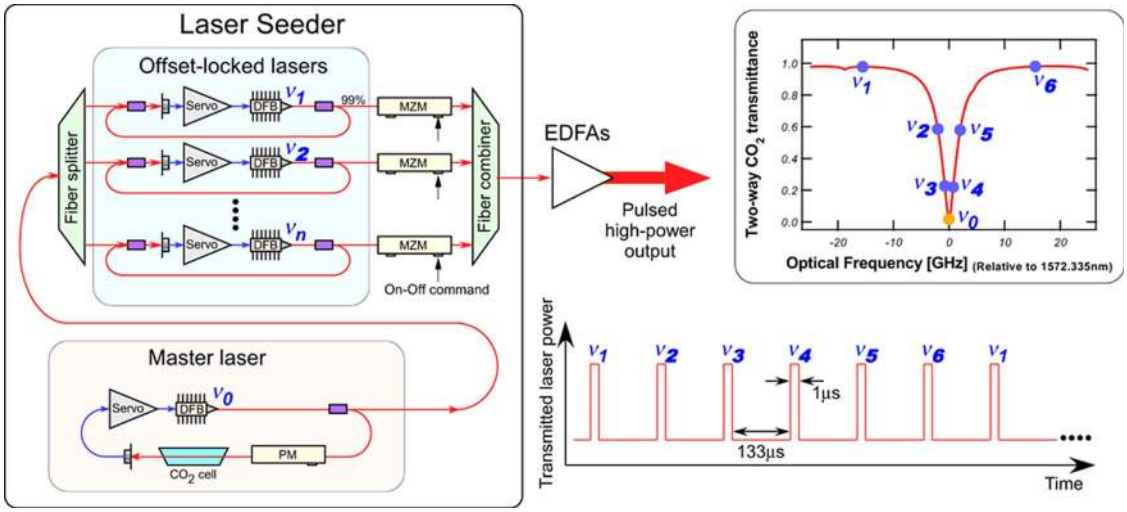

Fig. 1. (Color online) Basic design concept for our CO_2 sounder transmitter. The laser seeder (left) is rapidly pulsed and switched among the six measurement laser frequencies to provide the wavelength-stepped pulse train (lower right) that is subsequently amplified by EDFAs. The amplified pulse-train is used to repeatedly measure at six points across the 1572.335 nm CO_2 absorption line (upper right).

optical frequency drift to 0.3 MHz, better than the ASCENDS requirement. We further offset locked four online DFB-LDs on the sides of the CO_2 line (ν_2 to ν_5 in Fig. 1), suppressing their frequency drifts to virtually the same submegahertz level of the master laser. The two offline DFB-LDs (ν_1 and ν_6) can tolerate much larger frequency drifts and thus were left to free run under stabilized temperatures and currents. The six DFB-LDs were externally modulated to generate the pulses and subsequently combined to produce the measurement pulse train as shown in Fig. 1 (lower right corner). The pulses in this combined output were ~1 μs wide, separated by ~133 μs. For space use, the off interval permits the pulses to completely clear the bottom 20 km of the atmosphere, eliminating the crosstalk from cloud scattering.

To suppress the crosstalk among the six wavelengths to < -32 dB, each modulator needs to have an >40 dB on/off extinction ratio (ER). This requirement was achieved with auto-biased telecom lithium-niobate (LN) Mach–Zehnder modulators (MZMs), to take advantage of their high reliability, compact size, and low power consumption. Based on these laser frequency locking and pulse modulation techniques, we have constructed a laser seeder for the CO_2 transmitter.

2. Absolute Frequency Locking

A. Absolute Locking Design Considerations

It is difficult to suppress the slow frequency drift to submegahertz by locking a laser frequency to an optical cavity. A molecular or atomic transition is thus preferred as the wavelength reference. Unfortunately, the well-known wavelength references for 1.5 μm lasers, such as C_2H_2 [14,15], CO [16], $H^{13}C^{14}N$ [17], and ^{87}Rb [18], do not have strong absorption lines near the 1572.335 nm CO_2 line selected for the measurement. Consequently, the 1572.335 nm CO_2 line becomes the reference of choice for the absolute wavelength locking.

We adopted an external frequency modulation (FM) technique [19] to lock the master laser frequency to the 1572.335 nm CO_2 line center. Similar to the well-known Pound–Drever–Hall technique [20], this external FM technique uses external phase modulation and phase-sensitive detection at an RF frequency to generate a frequency discriminating error signal. The FM technique effectively rejects noise (particularly low-frequency noise in the detector and the laser intensity) lying outside the RF detection bandwidth and allows frequency noise suppression in a wider control-loop bandwidth, resulting in better frequency stability than those obtained by locking directly to one side of a absorption line (e.g., 5 MHz rms to a similar CO_2 line as reported in [21]). A low-frequency counterpart of the RF FM technique, known as wavelength modulation (WM) technique [22], has also been widely used. The WM technique modulates the laser frequency internally at an audio frequency (AF) by dithering the laser diode injection current. In general, the WM technique adds undesirable amplitude and FMs to the laser output, suffers from higher noise at the AF, and results in smaller error signal slopes.

The predominant noise source with this FM technique is the time-varying residual amplitude modulation (RAM) arising from multipath interference (MPI), polarization misalignment, and other sources, particularly in the phase modulator [23,24]. Consequently, it is crucial to minimize the RAM in the phase modulator and the gas cell. The same FM technique had been used to lock lasers, for example, to $^{12}C_2H_2$ lines near 1.53 μm [25] and to CO_2 absorption lines near 2.05 μm [26,27]. In these previous experiments, bulk electro-optic (EO) phase modulators were commonly selected against wave-guided LN phase modulators due to the much higher RAM encountered in the latter. The telecom LN modulator technology has since been improved. We have selected compact telecom LN phase modulators for the present work to avoid the complexity of using free-space bulk components and high-voltage RF sources to drive EO modulators in space. The RAM in the LN phase modulators has been reduced to <0.04% peak-to-peak, low enough for our submegahertz frequency stability requirement.

To enhance the signal-to-noise ratio (S/N), strong and narrow absorption lines are sought for steep error signal slopes. Unfortunately, our CO_2 reference line (with a line strength $S_{ij} = 1.74\times 10^{-23}\ \mathrm{cm^{-1}/(mol\,cm^{-2})}$) is significantly weaker than, for example, CO_2 absorption lines near 2.05 μm ($S_{ij} \sim 2\times 10^{-22}\ \mathrm{cm^{-1}/(mol\,cm^{-2})}$) and $^{12}C_2H_2$ lines near 1.53 μm ($S_{ij} \sim 1\times 10^{-20}\ \mathrm{cm^{-1}/(mol\,cm^{-2})}$). Consequently, a much longer gas-cell path length is required for our reference CO_2 cell. We employed a multipass CO_2 cell to realize the long path length. To avoid mechanical instability and design complexity, no optical cavity was used to enhance the effective path length.

B. Absolute Locking Setup

Our absolute locking system is shown in Fig. 2. The master laser was a 40 mW single-mode (SM) PM DFB-LD with a narrow linewidth of <2 MHz (FRL15DCWD-A81-19070-B, OFS Fitel, LLC). It contains a built-in isolator with >35 dB isolation to prevent unwanted feedback. The master laser output was divided into two outputs using an SM PM fiber coupler. Ninety percent of the light was used to lock

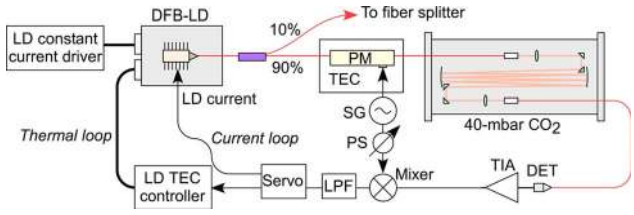

Fig. 2. (Color online) Absolute frequency locking setup for the master DFB-LD. DET, PIN detector; LPF, low-pass filter; PM, phase modulator; PS, phase shifter; SG, signal generator.

this master laser. The rest is used to offset lock slave DFB-LDs after being further split through a PM fiber splitter (discussed later). The 90% laser output was passed through a fiber-coupled, wave-guided 10 GHz LN phase modulator (PM-150-100-1-1-C2-I2-O2 APE, JDSU Corp.). To further reduce error signal drift due to the RAM, the case temperature of this LN phase modulator was stabilized with a thermoelectric cooler (TEC). The modulated laser beam was subsequently passed through a CO_2 absorption cell with a path length of 17 m and a CO_2 pressure of 40 mbar. The phase modulator was driven by a 125 MHz sinusoidal voltage at a modulation index of ~2.5, generating sidebands that are 125 MHz apart around the optical carrier. The transmitted laser beam was finally detected by a fiber-coupled InGaAs PIN photodiode. The detector current was AC-coupled to and amplified by a low-noise transimpedance amplifier (TIA). A demodulation circuit (i.e., mixer, phase shifter, and low pass filter) makes phase-sensitive detection of the amplified beatnote at 125 MHz, and produces an error signal proportional to the laser frequency deviation from the CO_2 line center. The loop servo feeds two signals back to the DFB-LD to stabilize its optical frequency: one slowly adapts the DFB-LD temperature through the TEC controller; the other rapidly adjusts the injection current through a resistor network [28] that adds the feedback on top of the constant bias current. The servo was controlled by an onboard microprocessor, which automatically finds the absorption peak and triggers switches in the servo circuit. Two identical absolute locking systems were built and the beatnote between the two independent lasers was used to measure the laser frequency noise.

Our CO_2 cell was carefully designed to minimize the MPI. Two spherical mirrors were placed inside a CO_2 chamber, forming a multipass optical delay line [29] with beam spots well separated on the mirrors. The laser beam was coupled in and out of the chamber through SM fibers hermetically sealed to the chamber, eliminating optical windows that could cause MPI. The high reflectivity of the protected, silver-coated mirrors resulted in a low cell insertion loss of ~5 dB (gas absorption excluded). The CO_2 cell pressure, modulation frequency and depth, and the phase shifter delay were optimized to maximize the slope of the error signal shown in Fig. 3.

C. DFB-LD Frequency Tuning Transfer Function

To facilitate the feedback loop servo design, the DFB-LD frequency tuning response to the injection current was measured (Fig. 4). In this measurement, a fiber Michelson interferometer (MI) was used as the frequency discriminator to detect frequency variations induced by a modulation voltage applied to the injection current feedback port of the DFB-LD. The MI was similar to that described in [30], and was auto-biased at a quadrature point using a control circuit. The delay time difference in the two arms of the MI was 3.2 ns. The small thermal impedance in the DFB-LD package resulted in a wide-tuning bandwidth of ~1 MHz. Allowing for a 30° phase margin for the feedback loop, this laser tuning response set an upper limit of ~800 kHz on our unity-gain loop bandwidth.

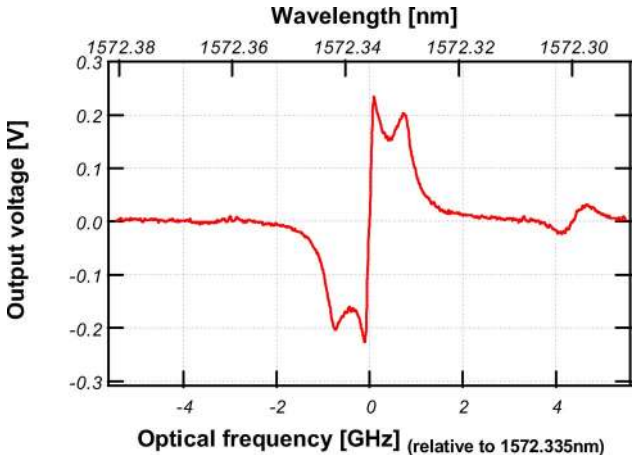

Fig. 3. (Color online) Error signal measured in the absolute frequency locking setup shown in Fig. 2. The depression at the positive and negative peaks of the error signal is attributed to the mixer saturation.

D. Master Laser Frequency Noise Measurements

Because the error signal does not reflect any frequency drifts caused by mechanisms that shift the frequency locking point (e.g., RAM and the noise in the detector), it is essential to measure the frequency drifts directly from the beatnote between two independent lasers (rather than from the error signal). The 10% output tapped from each laser (external to the locking loop) was used to produce the beatnote. In order to shift the beatnote away from zero frequency for better measurement sensitivity, one laser output was frequency up-shifted by 35 MHz using a fiber-coupled acousto-optic modulator. This frequency-shifted laser output was combined with the other one using a 3 dB SM PM fiber coupler, and the combined laser output was detected by a PIN photodiode. The instantaneous frequency of the beatnote from the detector was measured by a frequency counter at rates up to 200 Hz. As shown in Fig. 5, the

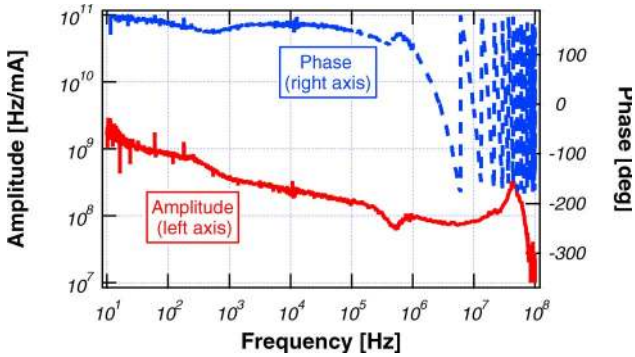

Fig. 4. (Color online) Frequency tuning response of the DFB-LDs as a function of the injection current modulation frequency.

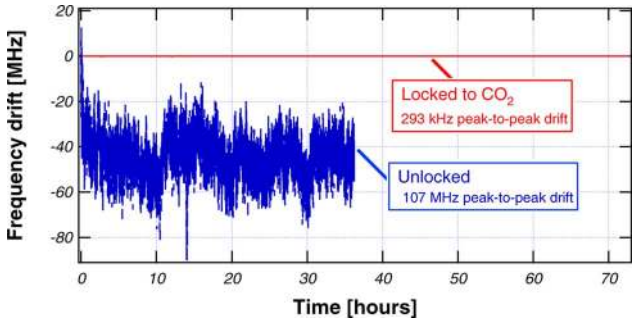

Fig. 5. (Color online) Optical frequency drifts of a DFB-LD measured from the beatnote between two equivalent and independent master lasers. The frequency drifts of each one of the two lasers locked to the 1572.335 nm CO_2 line were obtained by assuming equal and independent frequency noises from both. The unlocked frequency drifts were obtained by unlocking one of the two lasers.

frequency drift of a DFB-LD was suppressed to 293 kHz peak-to-peak (with a standard deviation of 59 kHz) at 0.8 s averaging time observed over 72 hours when locked to the 1572.335 nm CO_2 line. By contrast, the frequency drift was 107 MHz over 36 hours when the laser was unlocked.

Figure 6 shows measured frequency noise spectra (square-root of noise power spectral density) of the DFB-LDs when locked and unlocked. For slow noise frequencies up to 100 Hz, the spectra were derived from the beatnote measured with the frequency counter (as described above). The rest of the spectra were measured with a fiber MI similar to the one used for laser frequency tuning response measurements. To suppress seismic and acoustic disturbances, the MI was mechanically stabilized by vibration-isolating stages suspended in a vacuum chamber. As seen in Fig. 6, the frequency noise of the absolutely locked DFB-LD was suppressed within the 800 kHz unity-gain bandwidth, by a factor up to ~1000 for low frequency noise sources. The fractional Allan deviation of the two absolutely locked master DFB-LDs was measured to be $<3 \times 10^{-11}$ for a gating time up to 1000 s, as shown in Fig. 7. This

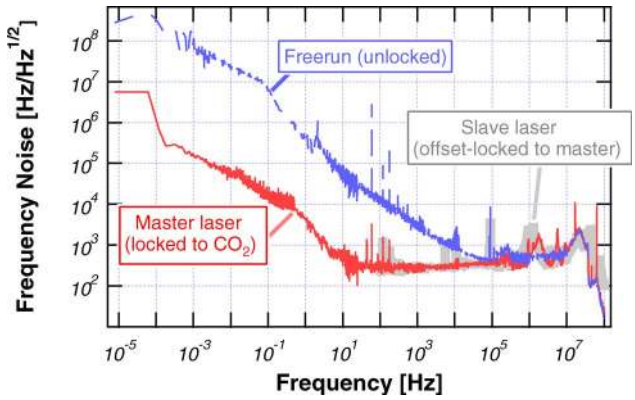

Fig. 6. (Color online) DFB-LD optical frequency noise spectra measured for: an unlocked laser; a master laser absolutely locked to a CO_2 cell using the setup shown in Fig. 2; and a slave laser offset locked to the master laser using the setup shown in Fig. 8.

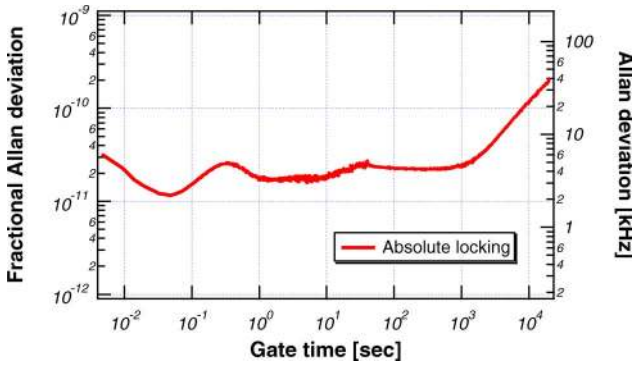

Fig. 7. (Color online) Allan deviation of the two absolutely locked master DFB-LDs.

stability is, for example, 300–2500× better than obtained by using the WM technique to lock lasers to H_2O lines ($S_{ij} \sim 10^{-22}\,\mathrm{cm}^{-1}/(\mathrm{mol\,cm}^{-2})$) [31].

3. Offset Frequency Locking

A. Offset Locking Setup

In order for the slave DFB-LDs to retain the frequency stability of the master laser, the fluctuation of the frequency offset must be suppressed to a small fraction of the frequency noise of the master laser. Various offset locking techniques have been developed to lock the frequency difference between two lasers [31–35]. Our offset locking setup, shown in Fig. 8, was based on the scheme described in [33], that appears to be most suitable to our purpose yet easy to implement with DFB-LDs.

The four online and two offline DFB-LDs were identical to the master DFB-LD. Referring to Fig. 1, we have offset locked two online DFB-LDs to ν_3 and ν_4 with frequency offsets of ± 755.2 MHz, and two other online DFB-LDs to ν_2 and ν_5 with frequency offsets of ± 2.014 GHz. The two free-running offline DFB-LDs (ν_1 and ν_6) were placed ± 15.6 GHz away from the CO_2 line center.

The beatnote between each slave laser and the master is frequency divided and subsequently phase locked to an RF reference signal. As shown in Fig. 8, 1% of the slave DFB-LD power was tapped off for offset locking and the remaining 99% was transmitted toward its MZM. Using an SM PM fiber splitter, the 10% light tapped from the master laser was further split into multiple fiber outputs, each with ~1% of the master laser power. The 1% slave laser power was

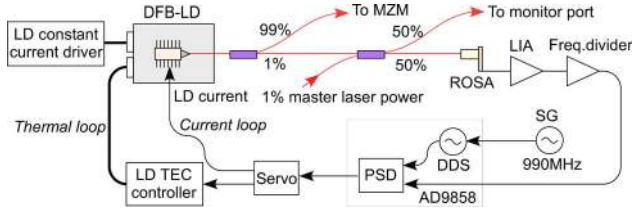

Fig. 8. (Color online) Offset frequency locking setup for the slave DFB-LDs: ROSA, receiver optical subassembly; LIA, limiting amplifier; DDS, direct digital synthesizer; PSD, phase sensitive detector.

mixed with the 1% master laser power using a 3 dB SM PM fiber coupler. The combined laser output was detected by a 10 GHz telecom receiver optical subassembly (ROSA) that consists of a PIN photodiode followed by an integrated TIA (ERM568RLC, JDSU Corp.). The sinusoidal beatnote detected by the ROSA was amplified by a limiting amplifier (LIA) and subsequently frequency divided by a digital frequency divider by a factor of 8 for 755.2 MHz offset, or 16 for 2.014 GHz offset. A digital phase-sensitive detector (PSD) was used to detect the phase difference between the divided beatnote and a precision electronic reference signal generated by a direct digital synthesizer (DDS), and to generate an error signal proportional to this phase difference. A commercial IC chip (AD9858, Analog Devices, Inc.) was used to provide both PSD and DDS functions. The servo provided feedback signals and frequency stabilized the slave DFB-LD in the same way as described for the master laser. Externally driven by a 990 MHz reference clock, the DDS output can be fast tuned with digital commands to produce the reference signal at desired frequencies, with great accuracy and flexibility. For the four online lasers, the reference signal was tuned to 94.4 MHz or 125.9 MHz for ±755.2 MHz or ±2.014 GHz offsets, respectively. The frequency divider, PSD, DDS, and servo circuits were controlled by a microcontroller, providing autotuning and auto-locking functions.

It should be noted that the error signal from the PSD is proportional to the integral of the laser frequency deviation, rather than to the frequency deviation itself, as is the case in the master laser locking setup. This was taken into account in the servo design. The carefully designed servo achieved the maximum unity-gain bandwidth of ~800 kHz for the slave laser as well. This bandwidth is sufficient for our CO_2 laser sounder system. The maximum frequency offset can be increased to ±20 GHz by replacing the PIN-TIA detector, the LIA, and the frequency divider with commercially available 20 GHz components.

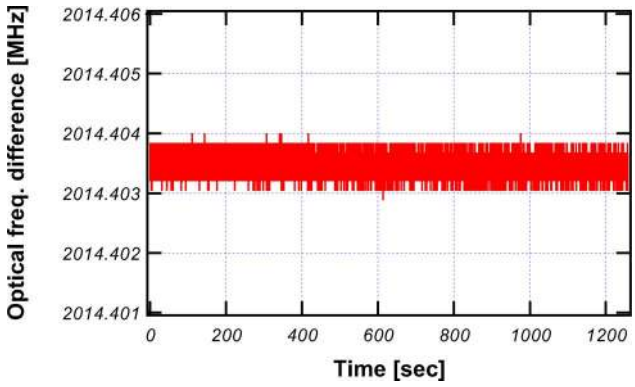

Fig. 9. (Color online) Optical frequency difference between a slave DFB-LD and a maser DFB-LD when the slave was locked to the master with 2.014 GHz frequency offset using a phase-locked loop shown in Fig. 8.

B. Slave Laser Frequency Noise Measurements

The frequency difference (beatnote) between the master and slave lasers was directly measured with a frequency counter at 200 Hz sampling rate (the result is shown in Fig. 9). When offset locked, the peak-to-peak fluctuation of the frequency offset was <1 kHz, a negligible fraction of the master laser frequency drift. We further found that most of the fluctuation came from the reference signal generated by the DDS. The frequency noise spectra of offset locked DFB-LDs were also measured in the same way as for the master laser, and were found to be essentially identical to that of the master laser (see Fig. 3). This means that a slave laser can be tuned to any wavelength across the CO_2 line with virtually identical absolute frequency stability as the master laser. Because the frequency divided beatnote (between the master and slave lasers) was phase locked to the RF reference signal, no constant deviation was found between the two. This means the offset frequency locking attains absolute accuracy without any DC bias error.

4. Seeder Pulse-Train Generation

A. Setup for Pulse-Train Generation

As shown in Fig. 10, the six lasers (ν_1–ν_6) were individually amplitude modulated by six MZMs and subsequently combined to produce the measurement pulse train. The *X*-cut LN MZMs (MXPE-LN-10-PD-P-P-FA-FA, Photline Technologies) have an intrinsic ER of >40 dB and were auto-biased at null points and pulsed with on/off RF signals. *X*-cut LN MZMs were selected to minimize the optical frequency chirping during the on/off modulation [36]. Standard MZM bias controllers typically add ~3 dB more off-state leakage, and this ER penalty becomes more severe at the low pulse rate (~1 kHz) for our application. This problem was solved with customized MZM bias controllers (Mini-MBC-1B, YY Labs Inc.). For each MZM, 1% MZM output was tapped out and fed to the bias card that biases the MZM automatically. The on/off ER was measured to be virtually the same as the intrinsic ER, with a negligible auto-bias ER penalty (<0.6 dB) even for slow pulse rates down to 1 kHz. The ER of the MZMs changes by >4 dB when the bias voltage changes polarity. The custom bias card permits bias polarity selection to pick the better null point. It would have been simpler to use the photodiode integrated into the MZM to feed the

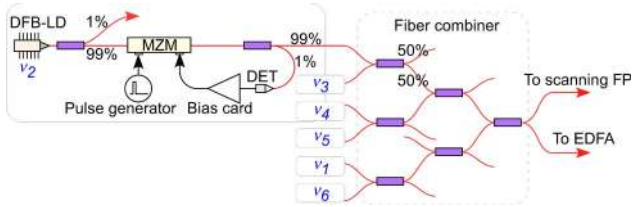

Fig. 10. (Color online) Setup to produce the measurement pulse train from the six online and offline DFB-LDs. DET, detector. The fiber combiner was built from cascaded 3 dB SM PM fiber couplers.

bias card. However, this arrangement resulted in an inferior ER, probably because the built-in detector sees the maximum light intensity (hence larger shot noise) when the MZM is biased at a null point.

The six MZMs were driven by one multichannel digital delay pulse generator that generates 1 μs pulses at 1.25 kHz for each MZM. All six laser pulse trains were combined using an SM PM fiber combiner built from cascaded 3 dB SM PM couplers. A proper time delay was set in the pulse generator for each MZM to maintain equal pulse separation of ~133 μs in the seeder output. The on/off ER for this combined seeder pulse train was better than 38 dB.

B. Laser Seeder Output Measurements

The optical spectrum of the seeder output was measured using a scanning plane–plane Fabry–Perot (FP) interferometer with ~60 GHz free spectral range. As shown in Fig. 11, frequency offsets relative to the CO_2 line center were indeed ±755.2 MHz, and ±2.014 GHz for the four online DFB-LDs and ~± 15.6 GHz for the two offline DFB-LDs. The spurious peaks in the spectrum were due to parasitic resonance in the plane–plane FP interferometer.

This combined seeder output was amplified by an SM PM EDFA preamplifier. Figure 12 shows pulse train waveforms measured before and after the preamplifier. The preamplifier output will be amplified by an EDFA power amplifier, and finally by an erbium–ytterbium planar waveguide power amplifier to boost the pulse energy to ~3 mJ as required for ASCENDS measurements. Because of the narrow linewidth and long pulse duration of the laser seeder, the stimulated Brillouin scattering (SBS) in the subsequent power amplifiers becomes a major challenge. The peak power in each power amplifier is limited by the SBS threshold that is well below thresholds of other nonlinear effects (e.g., self-phase modulation). The frequency stability and narrow linewidth of the laser seeder will thus be well preserved at the transmitter output. Because of the gain saturation in the power amplifiers, the top-hat pulse shape of our laser seeder would be distorted at the transmitter output to have lower power at the trailing edge than the leading edge. This distortion can be counteracted

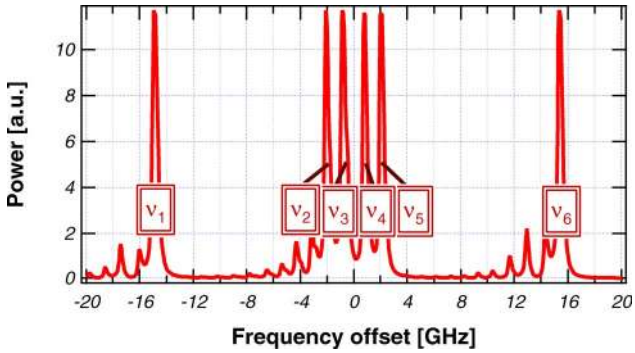

Fig. 11. (Color online) Optical spectrum of the seeder output measured by a scanning FP interferometer. The laser seeder stepped through the six fixed laser frequencies across the 1572.335 nm CO_2 line centered at 0 Hz offset in this plot.

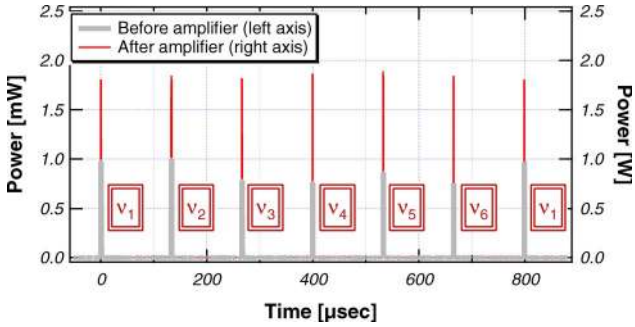

Fig. 12. (Color online) Combined seeder pulse train before and after being amplified by an EDFA preamplifier.

by predistortion of the input pulse shape [37]. This pulse predistortion can be accomplished by using one more LN MZM placed after the EDFA preamplifier. The on/off ER of the laser pulses can also be improved by gating the modulator to block the light between consecutive pulses, particularly the amplified spontaneous emission (ASE) from the preamplifier.

5. Discussion

A. Noise Sources in Absolute Frequency Locking

In our absolute locking setup, a sufficient laser power (>2 dBm) was detected by the PIN detector so that the detector shot noise and the TIA noise were negligible compared to the RAM-induced noise. When the detected laser power is above −6 dBm, the shot noise becomes larger than the ~8 pA/$\sqrt{\text{Hz}}$ equivalent input noise of the TIA, and the sum of both becomes a negligible fraction of the RAM-induced noise. RAM was the predominant noise source causing slow laser frequency drifts. We further noticed that the master laser locked to the CO_2 line center exhibited a constant frequency offset from the reference line center, typically a couple of hundred kilohertz. This offset is attributed to the constant component of the RAM and imperfect electronic components. It should also be noted that the 1572.335 nm atmospheric CO_2 line is pressure shifted from the CO_2 cell reference line by −0.25 MHz/Torr [38]. The overall offset can be calibrated with an external reference and corrected by shifting the offset locking reference frequencies.

B. CO_2 Cell Improvements

This laser seeder was constructed with telecom fiber-optic components, except for the bulky CO_2 cell we built for lab experiments. Much more compact CO_2 cells are required for flight missions. As an improvement, we replaced the bulky cell with a compact 18 m Herriott CO_2 gas cell (Model 5612, New Focus, Inc.) and achieved essentially the same absolute locking performance as described above. The laser beam was coupled in and out of the Herriott cell through a coated, wedged optical window in order to minimize MPI. The output beam was focused directly onto the PIN detector without fiber coupling, resulting in an overall cell insertion loss of ~9 dB (gas absorption excluded). Although the detected laser power was

reduced by ~4 dB due to this higher cell insertion loss, there appeared to be no S/N penalty.

It would be more desirable to build all-fiber CO_2 cells using hollow-core photonic crystal fibers (HC-PCFs) for size, weight, stability, and reliability advantages [39]. However, replacing the free-space CO_2 cell with an equivalent HC-PCF CO_2 cell in our setup resulted in much larger laser frequency drifts (~6 MHz peak-to-peak) than obtained with the free-space cell. Nevertheless, the spectra in both cases were comparable for noise frequencies above a few hertz. The slow frequency drifts persisted even when back reflections at both ends of the HC-PCF were suppressed and the temperature of the HC-PCF was stabilized. Such frequency drifts could not be detected by simply monitoring the error signal as described in [40], indicating a slow mechanism that shifts the error signal directly. The photonic bandgap HC-PCFs used to build these cells exhibit an oscillatory background in the transmission spectrum due to the effect of surface modes [41]. It appears that the large frequency drifts were driven by this time-varying background that falls on the gas absorption lines and mimics the gas absorption. This problem could be avoided by using nonbandgap-based HC-PCFs, in which the coupling between the hollow-core modes and the other modes is drastically reduced [42,43].

C. Adding More Wavelength Points

Recent results of our CO_2 laser sounder experiments [44,45] may indicate that more wavelength points (>10) are needed to correct for time-varying fringes in the lidar's frequency response. However, combining more lasers with lossy optical couplers (as shown in Fig. 10) would add more combining loss and crosstalk among wavelength channels. Higher combining loss will result in larger uncertainty in the measurement of the transmitter output pulse energy. The predominant noise in the pulse energy measurement is the beatnote between the ASE in EDFAs and the laser pulses detected by the monitoring PIN photodiode [46]. The measurement uncertainty arising from both the crosstalk and noise in the measurement of the transmitter pulse energy must be kept to a small fraction of the 0.08% total error budget. The stringent pulse-energy monitoring requirement can be met in our design by limiting the fiber combiner insertion loss to <11 dB, by using low-noise EDFAs, and by narrowing the electrical bandwidth of the monitoring detector to <10 MHz to reduce the ASE-pulse beating noise. However, our three-stage fiber combiner (shown in Fig. 10) already has an ~11 dB insertion loss and can combine eight lasers at most. Although more channels can still be combined by inserting additional EDFAs and modulators within the combiner to counteract the additional insertional losses and crosstalks, doing so will significantly complicate the laser seeder design.

It would thus be highly desirable to replace the multiple fixed-wavelength DFB-LDs and their modulators with one precision fast tunable laser and one modulator to drastically simplify the laser seeder architecture and to eliminate the combining loss and crosstalk. The frequency of this tunable laser needs to be accurately stepped through multiple points across the CO_2 line, as fast as ~100 μs per step and as precise as $\sim \pm 0.3$ MHz. This would significantly improve the S/N, reliability, flexibility, and reduce the power consumption, size, mass, and cost. More wavelength channels can be added without penalties.

We have recently started our development effort on the HC-PCF cells and the precision fast tunable lasers. We are also refining the present seeder system for field measurements. Further results will be reported as future progress is made.

6. Conclusions

A fiber-based pulsed laser seeder system was developed for measurements of global CO_2 mixing ratios to 1 ppmv precision. One master DFB laser diode has been frequency locked to the 1572.335 nm CO_2 line center using a FM technique, suppressing its peak-to-peak frequency drift to 0.3 MHz at 0.8 s averaging time over 72 hours. Slave DFB-LDs have been offset locked up to $\pm$7 GHz away from the master laser, stabilizing their absolute frequencies to virtually the same submegahertz precision of the master laser. Over 40 dB ER has been achieved in auto-biased MZMs to modulate continuous-wave lasers into pulses. Based on these techniques, the pulsed laser seeder was built to rapidly switch among six fixed wavelengths across the CO_2 line. The submegahertz frequency precision for online lasers satisfies the ASCENDS requirement.

The authors gratefully acknowledge A. Stummer at the University of Toronto for sharing technical details of his laser offset locking system through website postings. They are also indebted to Y. Yin at YY labs, Inc. for developing the custom MZM bias controllers, B. Merritt and the modulator design team at JDSU Corp. for helpful discussions on the RAM in the phase modulators, and J. Mao at NASA Goddard for providing atmospheric CO_2 absorption modeling results. R. DiSilvestre at NASA Goddard machine shop and F. Kimpel at Fibertek, Inc. contributed to the construction of the laser seeder system, and the authors are appreciative of their skillful assistance. This work was supported by the NASA Earth Science Technology Office Instrument Incubator Program and the NASA Goddard Internal Research and Development program.

References

1. J. R. Petit, J. Jouzel, D. Raynaud, N. I. Barkov, J.-M.Barnola, I. Basile, M. Bender, J. Chappellaz, M. Davis, G. Delaygue, M. Delmotte, V. M. Kotlyakov, M. Legrand, V. Y. Lipenkov, C. Lorius, L. Pépin, C. Ritz, E. Saltzman, and M. Stievenard, "Climate and atmospheric history of the past 420,000 years from the Vostok ice core, Antarctica," Nature **399**, 429–436 (1999).

2. R. J. Engelen, A. S. Denning, K. R. Gurney, and G. L. Stephens, "Global observations of the carbon budget: 1. Expected satellite capabilities for emission spectroscopy in the EOS and NPOESS eras," J. Geophys. Res. **106**, 20055–20068 (2001).
3. P. J. Rayner and D. M. O'Brien, "The utility of remotely sensed CO_2 concentration data in surface source inversions," Geophys. Res. Lett. **28**, 175–178 (2001).
4. C. E. Miller, D. Crisp, P. L. DeCola, S. C. Olsen, J. T. Randerson, A. M. Michalak, A. Alkhaled, P. Rayner, D. J. Jacob, P. Suntharalingam, D. B. A. Jones, A. S. Denning, M. E. Nicholls, S. C. Doney, S. Pawson, H. Boesch, B. J. Connor, I. Y. Fung, D. O'Brien, R. J. Salawitch, S. P. Sander, B. Sen, P. Tans, G. C. Toon, P. O. Wennberg, S. C. Wofsy, Y. L. Yung, and R. M. Law, "Precision requirements for space-based XCO_2 data," J. Geophys. Res. **112**, D10314 (2007).
5. M. Marquis and P. Tans, "Carbon crucible," Science **320**, 460–461 (2008).
6. Atmospheric Infrared Sounder, http://airs.jpl.nasa.gov.
7. Japan Aerospace Exploration Agency, http://www.jaxa.jp/projects/sat/gosat/index_e.html.
8. Space Studies Board, National Research Council, *Earth Science and Applications from Space: National Imperatives for the Next Decade and Beyond* (National Academies, 2007).
9. J. B. Abshire, H. Riris, G. Allan, X. Sun, S. R. Kawa, J. Mao, M. Stephen, E. Wilson, and M. A. Krainak, "Laser sounder for global measurement of CO_2 concentrations in the troposphere from space," in *Laser Applications to Chemical, Security and Environmental Analysis* of OSA Technical Digest Series (CD) (Optical Society of America, 2008), paper LMA4.
10. J. B. Abshire, H. Riris, G. R. Allan, C. J. Weaver, J. Mao, X. Sun, W. E. Hasselbrack, S. R. Kawa, and S. Biraud, "Pulsed airborne lidar measurements of atmospheric CO_2 column absorption," Tellus, Ser. B, Chem. Phys. Meteorol. **62**, 770–783 (2010).
11. J. Mao and S. R. Kawa, "Sensitivity studies for space-based measurement of atmospheric total column carbon dioxide," Appl. Opt. **43**, 914–927 (2004).
12. S. R. Kawa, J. Mao, J. B. Abshire, G. J. Collatz, X. Sun, and C. J. Weaver, "Simulation studies for a space-based CO_2 lidar mission," Tellus, Ser. B, Chem. Phys. Meteorol. **62**, 759–769 (2010).
13. G. Ehret, C. Kiemle, M. Wirth, A. Amediek, A. Fix, and S. Houweling, "Space-borne remote sensing of CO_2, CH_4, and N_2O by integrated path differential absorption lidar: a sensitivity analysis," Appl. Phys. B **90**, 593–608 (2008).
14. W. C. Swann and S. L. Gilbert, "Pressure-induced shift and broadening of 1510–1540 nm acetylene wavelength calibration lines," J. Opt. Soc. Am. B **17**, 1263–1270 (2000).
15. C. S. Edwards, H. S. Margolis, G. P. Barwood, S. N. Lea, P. Gill, G. Huang, and W. R. C. Rowley, "Absolute frequency measurement of a 1.5 mm acetylene standard by use of a combined frequency chain and femtosecond comb," Opt. Lett. **29**, 566–568 (2004).
16. S. L. Gilbert and W. C. Swann, "Standard reference materials: carbon monoxide absorption references for 1560 nm to 1630 nm wavelength calibration—SRM 2514 ($^{12}C^{16}O$) and SRM 2515 ($^{13}C^{16}O$)," NIST Special Publication 260-146 (National Institute of Standards and Technology, 2002).
17. W. C. Swann and S. L. Gilbert, "Line centers, pressure shift, and pressure broadening of 1530–1560 nm hydrogen cyanide wavelength calibration lines," J. Opt. Soc. Am. B **22**, 1749–1756 (2005).
18. A. Bruner, V. Mahal, I. Kiryuschev, A. Arie, M. A. Arbore, and M. M. Fejer, "Frequency stability at the kilohertz level of a rubidium-locked diode laser at 192.114 THz," Appl. Opt. **37**, 6410–6414 (1998).
19. G. C. Bjorklund, "Frequency-modulation spectroscopy: a new method for measuring weak absorptions and dispersions," Opt. Lett. **5**, 15–17 (1980).
20. R. W. P. Drever, J. L. Hall, F. V. Kowalski, J. Hough, G. M. Ford, A. J. Munley, H. Ward, "Laser phase and frequency stabilization using an optical resonator," Appl. Phys. B**31**, 97–105 (1983).
21. A. Amediek, A. Fix, M. Wirth, and G. Ehret, "Development of an OPO system at 1.57 μm for integrated path DIAL measurement of atmospheric carbon dioxide," Appl. Phys. B **92**, 295–302 (2008).
22. S. Schilt and L. Thévenaz, "Experimental method based on wavelength-modulation spectroscopy for the characterization of semiconductor lasers under direct modulation," Appl. Opt. **43**, 4446–4453 (2004).
23. E. A. Whittaker, M. Gehrtz, and G. C. Bjorklund, "Residual amplitude modulation in laser electro-optic phase modulation," J. Opt. Soc. Am. B **2**, 1320–1326 (1985).
24. N. C. Wong and J. L. Hall, "Servo control of amplitude modulation in frequency-modulation spectroscopy: demonstration of shot-noise-limited detection," J. Opt. Soc. Am. B **2**, 1527–1533 (1985).
25. F. Bertinetto, P. Gambini, R. Lano, and M. Puleo, "Frequency stabilization of DFB laser diodes to the P(3) line of acetylene at 1.52688 μm by external phase modulation," Proc. SPIE **1837**, 154–163 (1993).
26. M. W. Phillips, J. Ranson, G. D. Spiers, and R. T. Menzies, "Development of a coherent laser transceiver for the NASA CO_2 laser absorption spectrometer instrument," in *Conference on Lasers and Electro-Optics / International Quantum Electronics Conference and Photonic Applications Systems Technologies*, OSA Technical Digest Series (CD) (Optical Society of America, 2004), paper CMDD2.
27. G. J. Koch, J. Y. Beyon, F. Gibert, B. W. Barnes, S. Ismail, M. Petros, P. J. Petzar, J. Yu, E. A. Modlin, K. J. Davis, and U. N. Singh, "Side-line tunable laser transmitter for differential absorption lidar measurements of CO_2: design and application to atmospheric measurements," Appl. Opt. **47**, 944–956 (2008).
28. L. Hilico, D. Touahri, F. Nez, and A. Clairon, "Narrow-line, low-amplitude noise semiconductor laser oscillator in the 780 nm range," Rev. Sci. Instrum. **65**, 3628–3633 (1994).
29. I. A. Ramsay and J. J. Degnan, "A ray analysis of optical resonators formed by two spherical mirrors," Appl. Opt. **9**, 385–398 (1970).
30. J.-F. Cliche, M. Allard, and M. Têtu, "High-power and ultra-narrow DFB laser: the effect of linewidth reduction systems on coherence length and interferometer noise," Proc. SPIE **6216**, 62160C (2006).
31. R. Matthey, S. Schilt, D. Werner, C. Affolderbach, L. Thévenaz, and G. Mileti, "Diode laser frequency stabilisation for water-vapour differential absorption sensing," Appl. Phys. B **85**, 477–485 (2006).
32. S. Schilt, R. Matthey, D. Kauffmann-Werner, C. Affolderbach, G. Mileti, and L. Thévenaz, "Laser offset-frequency locking up to 20 GHz using a low-frequency electrical filter technique," Appl. Opt. **47**, 4336–4344 (2008).
33. A. Stummer, ""Chromamatic" laser tuning," http://www.physics.utoronto.ca/~astummer/pub/mirror/Projects/Archives/Laser%20Tuning/Laser%20Tuning.html.
34. R. T. Ramos and A. J. Seeds, "Fast heterodyne optical phase-lock loop using double quantum well laser diodes," Electron. Lett. **28**, 82–83 (1992).

35. U. Schünemann, H. Engler, R. Grimm, M. Weidemüller, and M. Zielonkowski, "Simple scheme for tunable frequency offset locking of two lasers," Rev. Sci. Instrum. **70**, 242–243 (1999).
36. F. Koyama and K. Iga, "Frequency chirping in external modulators," J. Lightwave Technol. **6**, 87–93 (1988).
37. A. Malinowski, K. T. Vu, K. K. Chen, J. Nilsson, Y. Jeong, S. Alam, D. Lin, and D. J. Richardson, "High power pulsed fiber MOPA system incorporating electro-optic modulator based adaptive pulse shaping," Opt. Express **17**, 20927–20937 (2009).
38. D. Sakaizawa, C. Nagasawa, T. Nagai, M. Abo, Y. Shibata, and M. Nakazato, "Measurement of pressure-induced broadening and shift coefficients of carbon dioxide absorption lines around 1.6 μm for using differential absorption lidar," Jpn. J. Appl. Phys. **47**, 325–328 (2008).
39. F. Benabid, F. Couny, J. C. Knight, T. A. Birks, and P. S. J. Russell, "Compact, stable and efficient all-fibre gas cells using hollow-core photonic crystal fibres," Nature **434**, 488–491 (2005).
40. P. Meras Jr., I. Y. Poberezhskiy, D. H. Chang, J. Levin, and G. D. Spiers, "Laser frequency stabilization for coherent lidar applications using novel all-fiber gas reference cell fabrication technique," presented at the 24th International Laser Radar Conference, Boulder, Colorado, 23 June 2008.
41. C. M. Smith, N. Venkataraman, M. T. Gallagher, D. Müller, J. A. West, N. F. Borrelli, D. C. Allan, and K. W. Koch, "Low-loss hollow-core silica/air photonic bandgap fibre," Nature **424**, 657–659 (2003).
42. F. Couny, F. Benabid, and P. S. Light, "Large-pitch kagome-structured hollow-core photonic crystal fiber," Opt. Lett. **31**, 3574–3576 (2006).
43. K. Knabe, S. Wu, J. Lim, K. A. Tillman, P. S. Light, F. Couny, N. Wheeler, R. Thapa, A. M. Jones, J. W. Nicholson, B. R. Washburn, F. Benabid, and K. L. Corwin, "10 kHz accuracy of an optical frequency reference based on $^{12}C_2H_2$-filled large-core kagome photonic crystal fibers," Opt. Express **17**, 16017–16026 (2009).
44. G. R. Allan, H. Riris, J. B. Abshire, X. Sun, E. Wilson, J. F. Burris, and M. A. Krainak, "Laser sounder for active remote sensing measurements of CO_2 concentrations," in *2008 IEEE Aerospace Conference* (IEEE, 2008).
45. J. Abshire, H. Riris, W. Hasselbrack, G. R. Allan, C. J. Weaver, and J. Mao, "Airborne measurements of CO_2 column absorption using a pulsed wavelength-scanned laser sounder instrument," in *Conference on Lasers and Electro-Optics/International Quantum Electronics Conference*, of OSA Technical Digest Series (CD) (Optical Society of America, 2009), paper CFU2.
46. P. C. Becker, N. A. Olsson, and J. R. Simpson, *Erbium-Doped Fiber Amplifiers: Fundamentals and Technology* (Academic, 1999).